

See discussions, stats, and author profiles for this publication at: <https://www.researchgate.net/publication/26271630>

Solution and Membrane-Bound Conformations of the Tandem C2A and C2B Domains of Synaptotagmin 1: Evidence for Bilayer Bridging

ARTICLE *in* JOURNAL OF MOLECULAR BIOLOGY · JULY 2009

Impact Factor: 4.33 · DOI: 10.1016/j.jmb.2009.06.007 · Source: PubMed

CITATIONS

36

READS

24

6 AUTHORS, INCLUDING:



Jeffrey Ellena

University of Virginia

45 PUBLICATIONS 1,305 CITATIONS

SEE PROFILE



NIH Public Access

Author Manuscript

J Mol Biol. Author manuscript; available in PMC 2010 July 31.

Published in final edited form as:

J Mol Biol. 2009 July 31; 390(5): 913–923. doi:10.1016/j.jmb.2009.06.007.

Solution and Membrane-Bound Conformations of the Tandem C2A and C2B Domains of Synaptotagmin 1: Evidence for Bilayer Bridging

Dawn Z. Herrick,

Department of Chemistry and Biophysics Program at the University of Virginia, Charlottesville, VA, 22904-4319

Weiwei Kuo,

Department of Chemistry and Biophysics Program at the University of Virginia, Charlottesville, VA, 22904-4319

Hao Huang,

Department of Chemistry and Biophysics Program at the University of Virginia, Charlottesville, VA, 22904-4319

Charles D. Schwieters,

Division of Computational Bioscience and Center for Information Technology at the National Institutes of Health, Bethesda, MD, 20892.

Jeffrey F. Ellena, and

Department of Chemistry and Biophysics Program at the University of Virginia, Charlottesville, VA, 22904-4319

David S. Cafiso*

Department of Chemistry and Biophysics Program at the University of Virginia, Charlottesville, VA, 22904-4319

Summary

Synaptotagmin 1 (syt1) is a synaptic vesicle membrane protein that functions as the Ca^{2+} -sensor in neuronal exocytosis. Here, site-directed spin labeling was used to generate models for the solution and membrane bound structures of a soluble fragment of syt1 containing its two C2 domains, C2A and C2B. In solution, distance restraints between the two C2 domains of syt1 were measured using double electron-electron resonance (DEER) and used in a simulated annealing routine to generate models for the structure of the tandem C2A-C2B fragment. The data indicate that the two C2 domains are flexibly linked and do not interact with each other in solution, with or without Ca^{2+} . However, the favored orientation is one where the Ca^{2+} -binding loops are oriented in opposite directions. A similar approach was taken for membrane associated C2A–C2B, combining both distances and bilayer depth restraints with simulated annealing. The restraints can only be satisfied if the Ca^{2+} and membrane binding surfaces of the domains are oriented in opposite directions so that C2A and C2B

© 2009 Elsevier Ltd. All rights reserved.

*Corresponding author email address cafiso@virginia.edu, tel: 434-924-3067, fax: 434-924-3567.

Publisher's Disclaimer: This is a PDF file of an unedited manuscript that has been accepted for publication. As a service to our customers we are providing this early version of the manuscript. The manuscript will undergo copyediting, typesetting, and review of the resulting proof before it is published in its final citable form. Please note that during the production process errors may be discovered which could affect the content, and all legal disclaimers that apply to the journal pertain.

are docked to opposing bilayers. The result suggests that syt1 functions to bridge across the vesicle and plasma membrane surfaces in a Ca^{2+} -dependent manner.

Keywords

Site-directed spin labeling; EPR spectroscopy; membrane fusion; protein-membrane interactions; calcium-binding protein

Introduction

Neuronal exocytosis is a highly coordinated Ca^{2+} -triggered process that involves the fusion of synaptic vesicles with the pre-synaptic membrane. This fusion event is regulated and facilitated by a large number of proteins, including the SNARE proteins. The SNAREs comprise the conserved molecular core of the fusion machinery and form a helical bundle that acts to tether the vesicle to the plasma membrane^{1, 2, 3}. In the neuronal system, there is good evidence that synaptotagmin 1 (syt1) acts as the Ca^{2+} sensor for SNARE-mediated fusion^{4, 5, 6, 7}.

Synaptotagmin 1 (Figure 1) is a membrane protein with two C2 domains (C2A and C2B) that are anchored to the vesicle membrane by a transmembrane helix located near its N-terminus. The C2A and C2B domains bind Ca^{2+} , and they have been shown to bind membrane surfaces containing negatively charged lipid in a Ca^{2+} -dependent fashion so that their first and third Ca^{2+} -binding loops penetrate into the lipid bilayer^{8, 9, 10, 11, 12}. Synaptotagmin 1 also interacts with the SNARE complex, apparently in both Ca^{2+} -independent and Ca^{2+} -dependent modes^{3, 4, 5, 13}.

The mechanism by which syt1 triggers exocytosis is presently not understood. There is evidence that syt1 may trigger exocytosis by interacting with membranes, the SNARE proteins or both. For example, it has been proposed that syt1 acts by directly binding to and regulating the SNAREs¹⁴, or by binding to membranes and creating curvature strain within the bilayer¹⁵. There is also evidence to support the proposal that syt1 acts to bridge across the vesicle and plasma membranes, either through the C2B domain^{16, 17}, or by having the two C2 domains bind to opposing membranes^{18, 19}.

The structures of the individual C2 domains of syt1 (C2A and C2B) have been known for some time^{20, 21, 22, 23}; however, the orientations of the two domains, relative to each other, in solution or bound to bilayers is not known. Recently a high-resolution structure for a fragment of syt1 containing its two C2 domains (syt1C2AB) was determined by crystallography in the absence of Ca^{2+} ²⁴. In this crystal structure (Fig. 1b), the two C2 domains interact so that the Ca^{2+} -binding loops of C2A interact near the H_A helix on C2B that connects strands 7 and 8. This structure suggests that the two C2 domains might be designed to interact with each other in the absence of Ca^{2+} , resulting in an inactive or closed form. The membrane binding regions in this structure are also facing in roughly opposite directions, suggesting that syt1 may be designed to interact with different membrane surfaces. Evidence for a direct interaction between the two C2 domains in syt1C2AB has also been obtained by FRET, but in this case, Ca^{2+} appears to induce an association of the two domains²⁵. In contrast to these two studies, NMR spectra of the soluble syt1C2AB fragment suggest that the two domains do not interact with each other in solution¹⁶; however, there may be conditions, bound to membranes or bound to SNAREs, where the two domains associate.

In the present work, site-directed spin labeling and pulse EPR spectroscopy were used to measure distances between pairs of spin-labels where one spin label was incorporated into C2A and a second label into C2B. These EPR-derived distance constraints were used in combination with simulated annealing to generate structures for syt1C2AB. In solution, the data show that

the two C2 domains of syt1 are flexibly linked and sample a range of conformations; however, the average conformation is one where the membrane binding surfaces of C2A and C2B are oriented in opposite directions. When bound to membranes, EPR-derived distance and bilayer depth restraints can only be satisfied when the two domains are docked to opposing bilayers. We discuss the implications of these results, which suggest that the C2 domains of syt1 may be configured to bridge from the vesicle to the plasma membrane.

Results

EPR spectra are consistent with the high-resolution structures of C2A and C2B and do not show evidence for a close approach of these domains

Thirteen sets of double cysteine mutants of syt1C2AB were produced, with one cysteine site located in C2A and a second site located in C2B. These cysteines were derivatized with a methanethiosulfonate nitroxide to incorporate either the R1 or in a few cases, the R7 side chain (Fig. 2a). Shown in Fig. 2b are the continuous wave EPR spectra of these mutant pairs labeled with R1. The EPR spectra arising from pairs of loop sites, such as 173R1/304R1, result from nitroxides that are mobile on the ns time-scale, typical of the R1 label at exposed loop sites^{26, 27}. The broader spectra, such as those from 189R1/327R1 and 244R1/327R1, result from labels that are more restricted in their motion, typical of β -sheet regions²⁸.

The EPR spectra shown in Fig. 2b may be approximated by summing the spectra of the individual labeled sites without any line broadening. For pairs of labels that are closer than 20 Angstroms, continuous wave EPR spectra are broadened due to dipolar interactions^{29, 30}, and the spectra in Fig. 2b indicate that the distance between labels in C2A and C2B exceeds 20 Angstroms. The spectra are not significantly altered by the addition or removal of Ca^{2+} , indicating that the labels in C2A and C2B are never close. The slight decrease in normalized intensity that is seen in the presence of Ca^{2+} in some spectra (for example, 173R1/304R1) is not the result of a change in interspin distance, but is the result of a slight decrease in backbone dynamics of the loop sites upon Ca^{2+} binding^{9, 21}.

Distance measurements between C2A and C2B are characterized by broad distributions, consistent with a flexible linker

Pulse EPR techniques permit the measurement of weak dipolar interactions between pairs of spin labels, allowing both distances and distance distributions between labels to be estimated^{31, 32, 33, 34}. In the present work, the four pulse, double electron-electron resonance (DEER) experiment was used to measure dipolar interactions between the spin labeled pairs in Fig. 2b. Shown in Figure 3 are representative DEER signals obtained for 5 pairs of labels, where the background signal due to intermolecular spin interactions has been subtracted. These signals are time-dependent amplitudes of a spin echo, which is modulated at the frequency of the dipolar interaction. Also shown in Figure 3b are fits to these DEER signals assuming a Gaussian distribution of distances. A deconvoluted dipolar spectrum (Pake pattern), and the resulting Pake pattern from the fit are shown in Fig. 3c. In these cases, a simple Gaussian distribution provides an adequate fit to the data.

Nitroxides that are separated by a well-defined distance having a narrow distance distribution will yield DEER signals that oscillate. The DEER signals obtained from labels in syt1C2AB are dampened, indicating that there is a broad distance distribution between the interacting spins. The distances obtained from the 13 sets of double labeled mutants in solution in the presence of Ca^{2+} are shown in Table 1. These distances ranged from 33 to 60 Angstroms, where the standard deviations describing the Gaussian distributions that fit the data ranged from 5 to as large as 18 Angstroms.

Estimating and subtracting the intermolecular background from DEER signals can be problematic, particularly for the longer distances measured here³⁴. As indicated in Table 1, there is a substantial uncertainty in some of these distances, and several approaches were used to minimize this error and ensure that the background signals were as accurately subtracted as possible. First, the dipolar evolution time used in these experiments was varied and extended in several cases to longer than 4 μ s, to more accurately assess the background. This did not significantly alter the distance or the distribution. Second, the form of the background subtraction used was confirmed by running DEER experiments on syt1C2AB with a single spin label in either C2A or C2B. For these cases, no DEER signal was obtained following subtraction of the background.

The broad distance distributions seen in Table 1 might have several different origins. A number of the labeled sites are within the calcium-binding loops, and the mobility of these loops might be the source of the broad distributions. However, these loops are not highly mobile in the presence of Ca^{2+} and are resolved in the crystal structures. In addition, labels placed within the more highly structured β -sheet regions of the C2 domains give similar distributions (compare for example, 173/332 and 244/327). The broad distributions might be a result of varied rotameric states in the R1 side chain. For spin labels at protein surface sites, rotations about the 4th and 5th bonds linking the spin label to the protein backbone may make a large contribution to the distance distribution³⁰. These rotations may be dramatically limited by the use of the R7 side chain (Figure 2a)³⁵. Here, the incorporation of R7 in place of R1 did not significantly alter either the measured distance or the distance distribution, indicating that the R1 label rotamers are not the source of the distribution. As a result, the distributions likely reflect variability in the relative orientations of the two C2 domains, a conclusion that is consistent with recent work indicating that the protein segment linking C2A and C2B is unstructured in solution³⁶.

Ca^{2+} addition does not produce a significant structural change in syt1C2AB

Distances between C2A and C2B were measured for a number of spin pairs in the absence of Ca^{2+} . In most cases, the distances obtained do not differ, within experimental error, from those obtained in the presence of Ca^{2+} (see Table 1). One exception is the labeled pair, 234R1/304R1, where the distance increased 3 Å in the presence of Ca^{2+} . For this spin pair, the error in the distance is estimated to be approximately ± 2 Å, and the small change measured is probably significant. Since 234R1 lies at the apex of one of the Ca^{2+} -binding loops, we speculate that Ca^{2+} -binding may result in either a small change in loop position, or alter the rotameric state of the spin label. In all cases, the distance distributions remain broad and do not significantly change, indicating that a highly defined geometry between C2A and C2B does not exist either in the presence or absence of Ca^{2+} .

The most probable structure for syt1C2AB in solution is one where the two domains have opposite orientations

As described in Methods, the simulated annealing software package Xplor-NIH was used to generate a model for the most probable structure for Ca^{2+} -bound syt1C2AB in solution using the EPR derived restraints. This essentially involved a “docking” of C2A to C2B using several pieces of data. First, the thirteen mean distances obtained between C2A and C2B (Table 1) were used as restraints, using distributions centered about this mean (see Methods). Second, previous work on syt1C2AB identified sites 266 to 272 in the segment linking C2A to C2B as unstructured³⁶, and this segment was not assigned a secondary structure in the simulated annealing. Finally, the solution structures obtained by NMR^{21; 22} were used to fix the backbone configuration for C2A and C2B.

Shown in Figure 4a is a view of the ten lowest energy structures obtained by simulated annealing, and Figure 4b is an average structure derived from the 20 lowest energy structures. The simulated annealing indicates that there are a range of structures consistent with the distances and distance distributions, but several features in these structures are apparent. The average separation between the centers of the domains is approximately 40 Angstroms and the van der Waals surfaces of the two domains do not come into contact. In addition, the two domains are oriented so that the Ca^{2+} -binding loops and membrane binding surfaces on C2A and C2B are roughly aligned in opposite directions. The anti-parallel alignment and orientations of the two domains is similar to that seen in the crystal structure in the absence of Ca^{2+} 24 (Figure 1b), however, the two domains are not in contact.

The images in Fig. 4 represent the most populated and the lowest energy structures for the two domains obtained by simulated annealing, but as indicated by the broad distance ranges (Table 1) and CW spectra from the linker³⁶, these domains sample a range of configurations and do not have a fixed orientation relative to each other. The structures presented in Fig. 4 are obtained when the standard deviation (SD) of the Gaussian distance distribution is set to SD/1.5. As expected, including a larger or smaller fraction of the Gaussian distance distribution in the simulated annealing results in a set of structures with a larger or smaller RMSD, respectively (see Methods).

EPR data indicate that Syt1C2AB binds to two opposing bilayers

Distance measurements from C2A to C2B were also carried out for syt1C2AB bound to POPC:POPS bilayers, under conditions where both domains are known to be completely membrane associated¹⁰. The distances and distributions obtained for the membrane bound form are remarkably similar to those obtained in solution (Table 1). There are no dramatic changes in distance upon membrane binding, and the distribution of distances between labels on each C2 domain remains broad. The broad distributions indicate that the geometry between C2A and C2B retains a high degree of structural heterogeneity even upon membrane association, a conclusion that is consistent with previous work demonstrating that the linker connecting C2A with C2B is flexible when syt1C2AB is bound to POPC:POPS bilayers³⁶. However, the fact that the mean distances are similar for membrane and aqueous syt1C2AB suggests that the average configurations are similar in the two environments.

In addition to the inter-domain distances from DEER (Table 1), other restraints for membrane bound syt1C2AB included 21 point-to-plane depth restraints (Table 2). These depth restraints were determined by power saturating the EPR spectra of single R1 spin labels on either C2A or C2B as described previously to provide a measure of the distance from the label to the average position of the lipid phosphates¹⁰. The point-to-plane depth restraints included 18 depth restraints determined previously from regions around the Ca^{2+} -binding loops¹⁰, as well as three additional sites on C2A and C2B. Of particular interest are two sites that were chosen on C2B that are opposite the Ca^{2+} binding loops (Fig. 5a). Although they are opposite the membrane face of C2B¹², the measured depth parameters (Φ values) indicate that sites 283 and 285 lie close to the bilayer surface. In particular, 285R1 appears to be positioned at the level of the lipid phosphate. The EPR spectra obtained from 283R1 and 285R1 are shown in Fig. 5b. The spectrum from 285R1 is a result of rapid anisotropic motion and it exhibits a slight change upon membrane binding that may be result of a decrease in local polarity. Both 283 and 285 are near two conserved arginine residues at 398 and 399 (Fig. 5a) that have been proposed to interact with the bilayer surface¹⁷.

To generate membrane bound structures for syt1C2AB, the interdomain distances and signed point-to-plane depth restraints were incorporated into Xplor-NIH (available starting in version 2.22). Initially, a simultaneous docking of C2A and C2B to each other and to a single plane, representing the average position of the phosphates at the bilayer interface, was attempted (see

Methods). The result of this simulated annealing is not realistic and places large regions of C2B into the bilayer interior. Since the average solution structure in Fig. 4 and the power saturation data from C2B (Fig. 5) suggest that syt1C2AB might bind with each domain facing opposing bilayer surfaces, a second approach was taken where the Ca^{2+} binding loops of C2A and C2B were docked to opposing, parallel planes representing two bilayer surfaces. Remarkably, simulated annealing using two planes produced structures for C2AB that satisfied all the EPR-derived restraints, and the fits appeared to be optimal when the two bilayer surfaces were separated by approximately 40 to 43 Angstroms.

The structure obtained from simulated annealing using two planes is shown in Fig. 6a. Both the backbone of the first and third Ca^{2+} -binding loops of each domain are inserted into or contact membrane interfaces, and the orientation of the individual domains is similar to that found previously using only depth restraints¹⁰. However, the domains are bound to opposite surfaces and are oriented in a roughly antiparallel fashion relative to each other. The structure in Fig. 6a positions the polybasic surface of C2B in an orientation perpendicular to the bilayer surface, and the regions of C2A and C2B that are opposite the Ca^{2+} -binding loops are positioned near the opposing bilayer surfaces. This includes sites near R398 and R399 on C2B, which might be expected to interact electrostatically with the opposing bilayer surface.

It should be noted that the structure in 6a represents one of a family of structures. As was the case with the solution structure, C2A and C2B do not assume a highly defined orientation relative to each other in the membrane bound state, but remain flexibly linked.

Discussion

The C2 domains of synaptotagmin 1 have been identified as Ca^{2+} -sensors in neuronal exocytosis; however, the structural role of the two C2 domains is not known, and it is not clear whether there are conditions under which the two domains might associate. In the work described here, distances were measured between the two C2 domains of syt1 in a fragment containing both domains but lacking the transmembrane segment (syt1C2AB). The data indicate that the domains do not associate in solution and do not have a fixed orientation relative to each other. Furthermore, Ca^{2+} binding does not alter the relative orientation of the two domains and does not regulate their association or dissociation. These observations are consistent with EPR spectra, which show that the linker connecting the two domains is unstructured³⁶, and consistent with high-resolution NMR data indicating that the two domains are flexibly linked in solution¹⁶. The data do not support proposals that Ca^{2+} modulates the association of the two domains of synaptotagmin 1^{24; 25}.

Distance restraints obtained using site-directed spin labeling, were incorporated into Xplor-NIH and simulated annealing was used to generate models for solution and membrane associated forms of syt1C2AB. In solution, the most favored orientation for the C2A and C2B domains is one where the two domains are oriented in opposite directions (Fig. 4). This orientation resembles the crystal structure in the absence of Ca^{2+} , except that the two domains are not in contact²⁴. Although there is no permanent contact between the two domains, several features of syt1C2AB may promote this orientation. First, the C2 domains are highly polarized, and the electrostatic fields from the two domains may overlap and influence their mutual orientation.

Second, while the linker is unstructured, it may not be sufficiently long to permit completely random orientations between the two domains. Remarkably, the distances and distributions do not change significantly upon membrane association, indicating that syt1C2AB remains highly dynamic when membrane bound. Furthermore, the membrane bound structure that best fits the data is one where C2A and C2B are docked to opposing bilayers.

The structure presented in Fig. 6a provides strong evidence that one function of syt1 may be to bridge across two bilayers in a Ca^{2+} -dependent manner. Such a bridging function for syt1 is consistent with a number of observations. First, increasing the concentration of syt1C2AB beyond the levels used here for EPR will result in vesicle aggregation (data not shown). Second, there have been several recent reports, using light scattering and electron microscopy, describing syt1 induced aggregation and a close approach of bilayers. Some of this work was carried out under conditions similar to those used here. In one study, vesicle aggregation could be induced by C2B alone¹⁶, but in another, only the tandem fragment containing both C2A and C2B could promote vesicle association³⁷.

A model for how intact syt1 might bridge across two bilayers is shown in Fig. 6b. In this model C2B is bound to the plasma membrane surface and C2A to the vesicle membrane surface. The localization of the C2B Ca^{2+} -binding loops to the plasma membrane surface (rather than the vesicle surface) might be driven by the presence of PI(4,5)P₂ in the plasma membrane (which promotes C2B membrane binding⁸). The C2A domain is more closely tied to the vesicle membrane through the transmembrane segment, which might also force C2B to interact with the plasma membrane. The models shown in Figure 6 indicate that the regions of C2B and C2A that are opposite the Ca^{2+} -binding loops approach bilayer surfaces. We do not presently have data on C2A, but data obtained here indicate that sites on C2B, which are opposite the Ca^{2+} -binding region, are close to a bilayer surface when syt1C2AB is membrane bound. This site lies with a region in C2B that has been proposed to interact with bilayers and bridge C2B across two bilayers. This interaction might be mediated, in part, through two conserved arginine residues (R398, R399) that appear to be critical for syt1 function¹⁷.

There is evidence that the polybasic face of C2B interacts with the SNARE complex, and that a simultaneous interaction takes place between C2B, membranes, and SNAREs in the presence of Ca^{2+} ³⁸. The model in Fig. 6 orients the polybasic face of C2B so that it is exposed and aligned perpendicular to the bilayer surface where it might interact with the surface of the core SNARE complex. While this syt1-SNARE interaction is feasible given the model in Fig. 6, we do not presently know whether the syt1 orientation shown in Fig. 6 is maintained in the presence of SNAREs. Exactly how a syt1/SNARE interaction might trigger fusion is not clear. There is evidence that syt1 regulates fusion by controlling conformational changes in the SNAREs¹⁴ or by displacing complexin from the SNARE complex³⁹. The data presented here suggest that syt1 might act simply to drive the vesicle and target membranes closer together in the presence of Ca^{2+} , an event that could alter the configuration of the SNAREs, perhaps driving them to a fusion competent state.

In a recent study of SNARE mediated vesicle fusion, full-length syt1 was shown to accelerate fusion when it interacted in a trans fashion, with C2B bound to the target¹⁸. Although it is not presently clear how a bridging function would promote fusion, a number of models seem plausible. As indicated above, bridging the vesicle and target membranes might alter the configuration of the SNAREs; in addition, it might facilitate formation of the fusion pore, as suggested previously¹⁷. By bringing two opposing bilayers together, syt1 might help stabilize the two bilayers, which must curve as a hemifusion intermediate is formed. Previous work indicates that syt1 promotes positive bilayer curvature, and conceivably, this ability to bridge bilayers might work together with a tendency to curve lipid bilayers to drive membrane fusion.

In summary, the data presented here indicate that the two C2 domains in syt1 are flexibly linked under a wide range of conditions. However, a highly populated configuration is one where the Ca^{2+} -binding regions face in roughly opposite directions. When bound to bilayers in the presence of Ca^{2+} , EPR-derived distance and bilayer depth restraints can only be satisfied if C2A and C2B bridge across two bilayers. In general, C2 domain containing proteins appear to be involved in a wide range of membrane trafficking and membrane repair processes. Many

of these membrane proteins contain multiple C2 domains. In addition to the synatotagmins, the tricalbins, copines, and ferlins^{40; 41; 42} are membrane anchored proteins that possess up to 6 or more C2 domains. The molecular function of these multiple domains has not yet been determined, but the results presented here on syt1 suggest that the C2 domains on these related proteins may also be flexibly linked. Since bilayers are highly dynamic structures, the inherent conformational flexibility between the two linked C2 domains of syt1 may be critical for recognizing and binding to opposing bilayer surfaces.

Materials and Methods

Mutagenesis, Protein Expression and Purification

DNA of rat syt1 (P21707), was obtained from Dr. Carl Creutz (Pharmacology Department, University of Virginia) in the pGEX-KG vector encoding amino acid residues 96–421 (syt1C2AB)⁴³. All DNA modifications followed published protocols⁴⁴. The single native cysteine residue at position 277 was mutated to alanine by typical polymerase chain reaction (PCR) strategies. A QuickChange Site-Directed Mutagenesis Kit (Stratagene, La Jolla, CA) was used to produce double-cysteine mutants of C2AB, and all cysteine substitutions were confirmed by DNA sequencing.

The expression and purification syt1C2AB was carried out as described previously¹⁰. Following affinity purification, steps were taken to remove residual GST and thrombin, and an additional anion exchange step was added to remove nucleic acid contaminants associated with the protein¹². Synaptotagmin 1 C2AB prepared in this manner, binds Tb³⁺ (a Ca²⁺ analog), membranes, and appears to be correctly folded as indicated by CD spectroscopy and FTIR^{10; 36}. Directly following anion exchange chromatography, pure fractions of syt1C2AB double mutants were spin-labeled as described previously using the sulfhydryl reactive spin label MTSL, (1-oxy-2,2,5,5-tetramethylpyrroline-3-methyl) methanethiosulfonate¹⁰. In a few cases, the 4-Bromo-(1-oxy-2,2,5,5-tetramethylpyrroline-3-methyl) methanethiosulfonate was incorporated. All labels were obtained from Toronto Research Chemicals (North York, ON, Canada)

Large Unilamellar Vesicles

1-palmitoyl-2-oleoyl-*sn*-glycero-3-phosphocholine (POPC) and 1-palmitoyl-2-oleoyl-*sn*-glycero-3-phosphoserine (POPS) (Avanti Polar Lipids, Alabaster, AL) were used to prepare large unilamellar vesicles (LUVs) with a POPC:POPS ratio of 3:1 as described previously⁹.

Electron Paramagnetic Resonance (EPR) Measurements

Continuous wave X-band EPR measurements were performed on 8 µL of sample loaded into glass capillaries with 0.60 mm i.d. × 0.84 mm o.d. (Fiber Optic Center, Inc., New Bedford, MA). Spin-labeled samples of double labeled Syt1C2AB mutants contained protein concentrations that varied from 100–185 µM in the presence (1mM Ca²⁺) or absence of calcium (5mM EGTA). EPR spectra were obtained on a modified Varian E-line 102 series X-band spectrometer with a loop gap resonator (Medical Advances, Milwaukee, WI). All spectra were taken at 2 mW incident microwave power and 1 G modulation amplitude. Scan range was 100 Gauss. For comparison, all spectra were normalized within a plot.

Pulse-EPR measurements were performed on 25–30 µL of sample loaded into quartz capillaries with 2.00 mm i.d. × 2.40 mm o.d. (Fiber Optic Center, Inc., New Bedford, MA). Spin-labeled samples of double labeled Syt1C2AB mutants contained protein concentrations that varied from 80–130 µM in the presence (1mM Ca²⁺) or absence of calcium (5mM EGTA), or in the presence of 3:1 POPC:POPS LUVs (25mM) and 1mM Ca²⁺. Samples of syt1C2AB in solution

contained 30% v/v glycerol, while samples of membrane-bound Syt1C2AB contained 5–22.5% v/v glycerol.

DEER samples were flash frozen in liquid nitrogen and the data were recorded at 78K on a Bruker Elexsys-E580 spectrometer fitted with an ER4118X-MS3 or -MS2 split ring resonator (Bruker Biospin, Billerica, MA). Data were acquired using a four-pulse DEER sequence⁴⁵ with a 16 ns $\pi/2$ and two 32 ns π observe pulses separated by a 32 ns π pump pulse. The dipolar evolution times were typically 2.2 μ s, with several samples taken out to 4.0 μ s. The pump frequency was set to the center maximum of the nitroxide spectrum and the observer frequency was set to the low field maximum, typically 65–70 MHz higher.

The phase-corrected dipolar evolution data were processed assuming a 3D background and Fourier Transformed, and the distance distributions were obtained with Gaussian fits using either the DeerAnalysis2006.1 package⁴⁶ or a LabView Program generously provided by Dr. Christian Altenbach (UCLA).

General structure calculation methods

Structures were calculated by using an Xplor-NIH simulated annealing procedure similar to that used previously for protein-protein docking^{47; 48}. The starting coordinates are from the high-resolution NMR structures of C2A (residues 140–267) and C2B (residues 272–419) (PDB ID: 1BYN and 1K5W, respectively^{21; 22}). At all stages the domains can rotate and translate but the relative coordinates of these atoms are held fixed. The spin-labeled side chains were subjected to molecular dynamics and energy minimization to a limited degree.

First, spin label side chains were appended at appropriate locations and the first two dihedral angles from the backbone for R1, X₁ and X₂, were set to -60° ⁴⁹. This is followed by simulated annealing with no experimental restraints during which the backbone structure of each domain and the first 5 atoms of each spin label side chain were fixed (to maintain X₁, X₂ = -60°), while other side chain atoms were allowed to find reasonable conformations. This provided starting structures for annealing with experimental restraints during which the entire spin label side chain conformations were fixed in addition to the C2 domain backbones. The structures are not very sensitive to the rotameric states chosen, however, if the R1 configurations are not set prior to the application of the interdomain restraints, unrealistic orientations of the spin labeled side-chains are generated. With this starting structure, the domain-domain restraints and domain-plane restraints (see below) provide the necessary translational and orientational information to orient the domains accurately, provided that no significant changes in the backbone of the domains occur upon membrane-binding.

The coordinates of average structures were obtained by averaging the coordinates of twenty individual lowest energy simulated annealing structures (out of one hundred generated structures) best fitted to each other. Structures were visualized and analyzed and figures were generated with the program PyMOL (DeLano Scientific LLC, Palo Alto, CA).

Modeling the Conformation of Syt1 C2AB

Thirteen inter-spin distances were used as input for an Xplor-NIH simulated annealing protocol^{47; 48} to determine the relative conformation of Ca²⁺-bound C2AB in solution. Starting C2AB structures for simulated annealing were obtained by appending the four missing residues of the linker region (E268-E269-Q270-E271) to the high-resolution NMR structures of C2A (residues 140–267) and C2B (residues 272–419) (PDB ID: 1BYN and 1K5W, respectively). Positions 173, 189, 199, 213, 234, 244 of C2A and 283, 285, 304, 327, 332, 353, 367 of C2B were mutated in silico to Cys and MTSL side chains were attached with the Xplor-NIH addAtoms.py script. Simulated annealing was performed as described above. The uncertainty

in the inter-spin distances was set using two thirds of the standard deviation (SD) of the distance distribution for the result shown in Fig. 4. Widening or narrowing the distance distribution to 1 SD or SD/3 produced a greater or narrower range of structures with RMSDs of 9.68 ± 4.86 , and 1.79 ± 1.54 Angstroms, respectively.

Membrane Docking of the Syt1 C2 domains

The position of syt1 C2A and C2B relative to each other and to the bilayer plane was determined similarly to the approach described above, except that twenty-one spin label depths (point-to-plane distances) and twelve inter-spin membrane-bound distances were used as input for standard Xplor-NIH restrained simulated annealing and energy minimization protocols^{47; 48}. Positions 171, 173, 174, 189, 199, 202, 213, 231, 234, 236, 239, 244 of C2A and 283, 285, 300, 304, 305, 306, 327, 332, 334, 353, 367, 368, 369, 370 of C2B were mutated in silico to Cys and MTSL side chains were attached with the Xplor-NIH addAtoms.py script. Eighteen depth parameters (Φ), from EPR power saturation as described previously, and three previously unpublished, were used to determine the distance (x) of the spin label from a bilayer plane using an empirically derived equation, where A , B , C , and D have values of 3.4, 0.11, 8.56, and 1.1, respectively¹⁰. The python Xplor-NIH plane distance potential (planeDistPot) was used to restrain the distances between the spin label nitrogen atoms and the phospholipid phosphate plane. The uncertainty in the depths was set according to the distance range determined from the empirically derived calibration curve. Similar approaches were used to dock the C2 domains to one or two planes, the only difference being that when two planes were used depth restraints were assigned to one of the two planes.

Abbreviations used

EPR, electron paramagnetic resonance spectroscopy; DEER, double electron-electron resonance; POPC, palmitoyloleoylphosphatidylcholine; POPS, palmitoyloleoylphosphatidylserine; R1 and R7, spin-labeled side chains produced by derivatization of a cysteine with a methanethiosulfonate spin label; RMSD, root mean square deviation; SD, standard deviation; SDSL, site-directed spin labeling; syt1, synaptotagmin 1; syt1C2AB, soluble fragment of syt1 containing the C2A and C2B domains.

Acknowledgements

This work was supported by a grant from the National Institutes of Health, NIGMS, GM 072694, and by the Intramural Research Program of the NIH (to CDS).

References

1. Rothman JE. Mechanisms of intracellular protein transport. *Nature* 1994;372:55–63. [PubMed: 7969419]
2. Jahn R, Lang T, Suhof TC. Membrane Fusion. *Cell* 2003;112:519–533. [PubMed: 12600315]
3. Sudhof TC. The synaptic vesicle cycle. *Annual Review of Neuroscience* 2004;27:509–547.
4. Chapman ER. How does synaptotagmin trigger neurotransmitter release? *Annu Rev Biochem* 2008;77:615–641. [PubMed: 18275379]
5. Rizo J, Chen X, Arac D. Unraveling the mechanisms of synaptotagmin and SNARE function in neurotransmitter release. *Trends Cell Biol* 2006;16:339–350. [PubMed: 16698267]
6. Jackson MB, Chapman ER. Fusion Pores and Fusion Machines in Ca²⁺-Triggered Exocytosis. *Annual Review of Biophysics and Biomolecular Structure* 2006;35:135–160.
7. Jahn R, Scheller RH. SNAREs - engines for membrane fusion. *Nature Reviews Molecular Cell Biology* 2006;7:631–643.

8. Bai J, Tucker WC, Chapman ER. PIP₂ increases the speed of response of synaptotagmin and steers its membrane-penetration activity toward the plasma membrane. *Nature Structural & Molecular Biology* 2004;11:36–44.
9. Frazier AA, Roller CR, Havelka JJ, Hinderliter A, Cafiso DS. Membrane-Bound Orientation and Position of the Synaptotagmin I C2A Domain by Site-Directed Spin Labeling. *Biochemistry* 2003;42:96–105. [PubMed: 12515543]
10. Herrick DZ, Sterbling S, Rasch KA, Hinderliter A, Cafiso DS. Position of synaptotagmin I at the membrane interface: cooperative interactions of tandem C2 domains. *Biochemistry* 2006;45:9668–9674. [PubMed: 16893168]
11. Hui E, Bai J, Chapman ER. Ca²⁺-triggered simultaneous membrane penetration of the tandem C2-domains of synaptotagmin I. *Biophys J* 2006;91:1767–1777. [PubMed: 16782782]
12. Rufener E, Frazier AA, Wieser CM, Hinderliter A, Cafiso DS. Membrane-Bound Orientation and Position of the Synaptotagmin C2B Domain Determined by Site-Directed Spin Labeling. *Biochemistry* 2005;44:18–28. [PubMed: 15628842]
13. Brunger AT. Structure and function of SNARE and SNARE-interacting proteins. *Q Rev Biophys* 2005;38:1–47. [PubMed: 16336742]
14. Bhalla A, Chicka MC, Tucker WC, Chapman ER. Ca(2+)-synaptotagmin directly regulates t-SNARE function during reconstituted membrane fusion. *Nat Struct Mol Biol* 2006;13:323–330. [PubMed: 16565726]
15. Martens S, Kozlov MM, McMahon HT. How Synaptotagmin Promotes Membrane Fusion. *Science* 2007;316:1205–1208. [PubMed: 17478680]
16. Arac D, Chen X, Khant HA, Ubach J, Luttko SJ, Kikkawa M, Johnson AE, Chiu W, Sudhof TC, Rizo J. Close membrane-membrane proximity induced by Ca(2+)-dependent multivalent binding of synaptotagmin-1 to phospholipids. *Nat Struct Mol Biol* 2006;13:209–217. [PubMed: 16491093]
17. Xue M, Ma C, Craig TK, Rosenmund C, Rizo J. The Janus-faced nature of the C(2)B domain is fundamental for synaptotagmin-1 function. *Nat Struct Mol Biol* 2008;15:1160–1168. [PubMed: 18953334]
18. Stein A, Radhakrishnan A, Riedel D, Fasshauer D, Jahn R. Synaptotagmin activates membrane fusion through a Ca²⁺-dependent trans interaction with phospholipids. *Nat Struct Mol Biol* 2007;14:904–911. [PubMed: 17891149]
19. Connell E, Giniatullina A, Lai-Kee-Him J, Tavare R, Ferrari E, Roseman A, Cojoc D, Brisson AR, Davletov B. Cross-linking of phospholipid membranes is a conserved property of calcium-sensitive synaptotagmins. *J Mol Biol* 2008;380:42–50. [PubMed: 18508081]
20. Sutton RB, Davletov BA, Berghuis AM, Sudhof TC, Sprang SR. Structure of the first C2 domain of synaptotagmin I: A novel Ca²⁺/phospholipid-binding fold. *Cell* 1995;80:929–938. [PubMed: 7697723]
21. Shao X, Fernandez I, Sudhof TC, Rizo J. Solution structures of the Ca²⁺-free and Ca²⁺-bound C2A domain of synaptotagmin I: does Ca²⁺ induce a conformational change? *Biochemistry* 1998;37:16106–16115. [PubMed: 9819203]
22. Fernandez I, Arac D, Ubach J, Gerber SH, Shin O, Gao Y, Anderson RG, Sudhof TC, Rizo J. Three-dimensional structure of the synaptotagmin 1 C2B-domain: synaptotagmin 1 as a phospholipid binding machine. *Neuron* 2001;32:1057–1069. [PubMed: 11754837]
23. Cheng Y, Sequeira SM, Malinina L, Tereshko V, Sollner TH, Patel DJ. Crystallographic identification of Ca²⁺ and Sr²⁺ coordination sites in synaptotagmin I C2B domain. *Protein Sci* 2004;13:2665–2672. [PubMed: 15340165]
24. Fuson KL, Montes M, Robert JJ, Sutton RB. Structure of Human Synaptotagmin 1 C2AB in the Absence of Ca²⁺ Reveals a Novel Domain Association. *Biochemistry* 2007;46:13041–13048. [PubMed: 17956130]
25. Garcia RA, Forde CE, Godwin HA. Calcium triggers an intramolecular association of the C2 domains in synaptotagmin. *Proc Natl Acad Sci U S A* 2000;97:5883–5888. [PubMed: 10811903]
26. Isas JM, Langen R, Haigler HT, Hubbell WL. Structure and dynamics of a helical hairpin and loop region in annexin 12: a site-directed spin labeling study. *Biochemistry* 2002;41:1464–1473. [PubMed: 11814339]

27. McHaourab HS, Lietzow MA, Hideg K, Hubbell WL. Motion of spin-labeled side chains in T4 lysozyme. Correlation with protein structure and dynamics. *Biochemistry* 1996;35:7692–7704. [PubMed: 8672470]
28. Lietzow MA, Hubbell WL. Motion of spin label side chains in cellular retinol-binding protein: correlation with structure and nearest-neighbor interactions in an antiparallel beta-sheet. *Biochemistry* 2004;43:3137–3151. [PubMed: 15023065]
29. Rabenstein MD, Shin YK. Determination of the distance between two spin labels attached to a macromolecule. *Proc Natl Acad Sci U S A* 1995;92:8239–8243. [PubMed: 7667275]
30. Altenbach C, Oh KJ, Trabanino RJ, Hideg K, Hubbell WL. Estimation of inter-residue distances in spin labeled proteins at physiological temperatures: experimental strategies and practical limitations. *Biochemistry* 2001;40:15471–15482. [PubMed: 11747422]
31. Prisner T, Rohrer M, MacMillan F. Pulsed EPR spectroscopy: biological applications. *Annu Rev Phys Chem* 2001;52:279–313. [PubMed: 11326067]
32. Jeschke G. Distance measurements in the nanometer range by pulse EPR. *Chemphyschem* 2002;3:927–932. [PubMed: 12503132]
33. Schiemann O, Prisner TF. Long-range distance determinations in biomacromolecules by EPR spectroscopy. *Q Rev Biophys* 2007;40:1–53. [PubMed: 17565764]
34. Jeschke G, Polyhach Y. Distance measurements on spin-labelled biomacromolecules by pulsed electron paramagnetic resonance. *Phys Chem Chem Phys* 2007;9:1895–1910. [PubMed: 17431518]
35. Columbus L, Kalai T, Jeko J, Hideg K, Hubbell WL. Molecular motion of spin labeled side chains in alpha-helices: analysis by variation of side chain structure. *Biochemistry* 2001;40:3828–3846. [PubMed: 11300763]
36. Huang H, Cafiso DS. Conformation and Membrane Position of the Region Linking the Two C2 Domains in Synaptotagmin 1 by Site-Directed Spin Labeling. *Biochemistry*. 2008
37. Connell E, Scott P, Davletov B. Real-time assay for monitoring membrane association of lipid-binding domains. *Anal Biochem* 2008;377:83–88. [PubMed: 18342614]
38. Dai H, Shen N, Arac D, Rizo J. A quaternary SNARE-synaptotagmin-Ca²⁺-phospholipid complex in neurotransmitter release. *J Mol Biol* 2007;367:848–863. [PubMed: 17320903]
39. Tang J, Maximov A, Shin OH, Dai H, Rizo J, Sudhof TC. A complexin/synaptotagmin 1 switch controls fast synaptic vesicle exocytosis. *Cell* 2006;126:1175–1187. [PubMed: 16990140]
40. Creutz CE, Snyder SL, Schulz TA. Characterization of the yeast tricalbins: membrane-bound multi-C2-domain proteins that form complexes involved in membrane trafficking. *Cell Mol Life Sci* 2004;61:1208–1220. [PubMed: 15141306]
41. Tomsig JL, Creutz CE. Copines: a ubiquitous family of Ca(2+)-dependent phospholipid-binding proteins. *Cell Mol Life Sci* 2002;59:1467–1477. [PubMed: 12440769]
42. Han R, Campbell KP. Dysferlin and muscle membrane repair. *Curr Opin Cell Biol* 2007;19:409–416. [PubMed: 17662592]
43. Damer CK, Creutz CE. Synergistic membrane interactions of the two C2 domains of synaptotagmin. *Journal of Biological Chemistry* 1994;269:31115–31123. [PubMed: 7983052]
44. Sambrook, J.; Fritsch, EF.; Maniatis, T. *Molecular Cloning: A Laboratory Manual*. Anonymous, editor. Plainview, N.Y: Cold Spring Harbor Press; 1989.
45. Pannier M, Veit S, Godt A, Jeschke G, Spiess HW. Dead-time free measurement of dipole-dipole interactions between electron spins. *J Magn Reson* 2000;142:331–340. [PubMed: 10648151]
46. Jeschke G, Chechik V, Ionita P, Godt A, Zimmermann H, Banham J, Timmel CR, Hilger D, Jung H. DeerAnalysis2006 - a comprehensive software package for analyzing pulsed ELDOR data. *Applied Magnetic Resonance* 2006;30:473–498.
47. Schwieters CD, Kuszewski JJ, Clore GM. Using Xplor-NIH for NMR Molecular Structure Determination. *Progress in Nuclear Magnetic Resonance Spectroscopy* 2006;48:47–62.
48. Schwieters CD, Kuszewski JJ, Tjandra N, Clore GM. The Xplor-NIH Molecular Structure Determination Package. *Journal of Magnetic Resonance* 2003;160:65–73. [PubMed: 12565051]
49. Guo Z, Cascio D, Hideg K, Hubbell WL. Structural determinants of nitroxide motion in spin-labeled proteins: solvent-exposed sites in helix B of T4 lysozyme. *Protein Sci* 2008;17:228–239. [PubMed: 18096642]

50. Frazier AA, Wisner MA, Malmberg NJ, Victor KG, Fanucci GE, Nalefski EA, Falke JJ, Cafiso DS. Membrane Orientation and Position of the C2 Domain from cPLA₂ by Site-Directed Spin Labeling. *Biochemistry* 2002;41:6282–6292. [PubMed: 12009889]

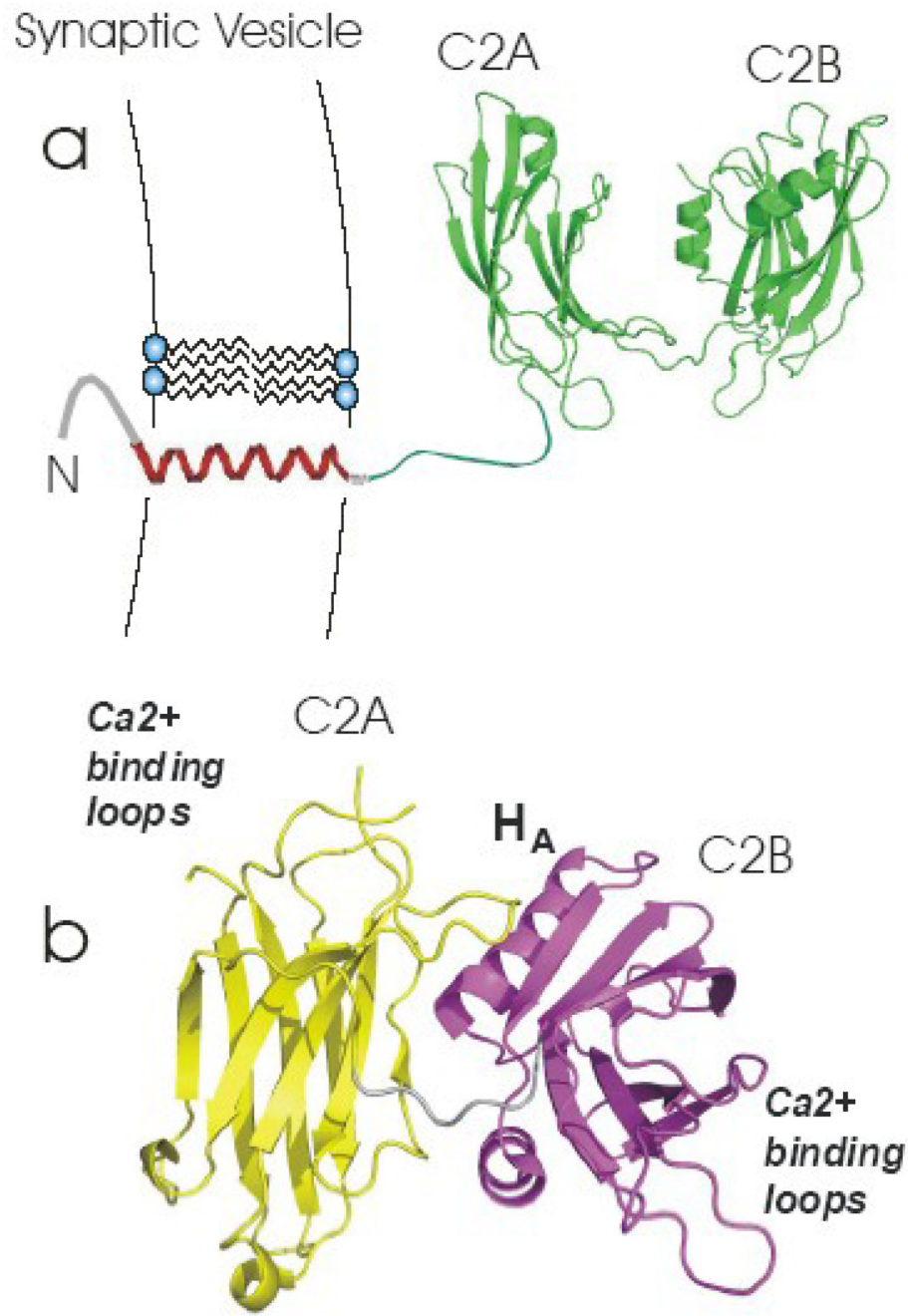
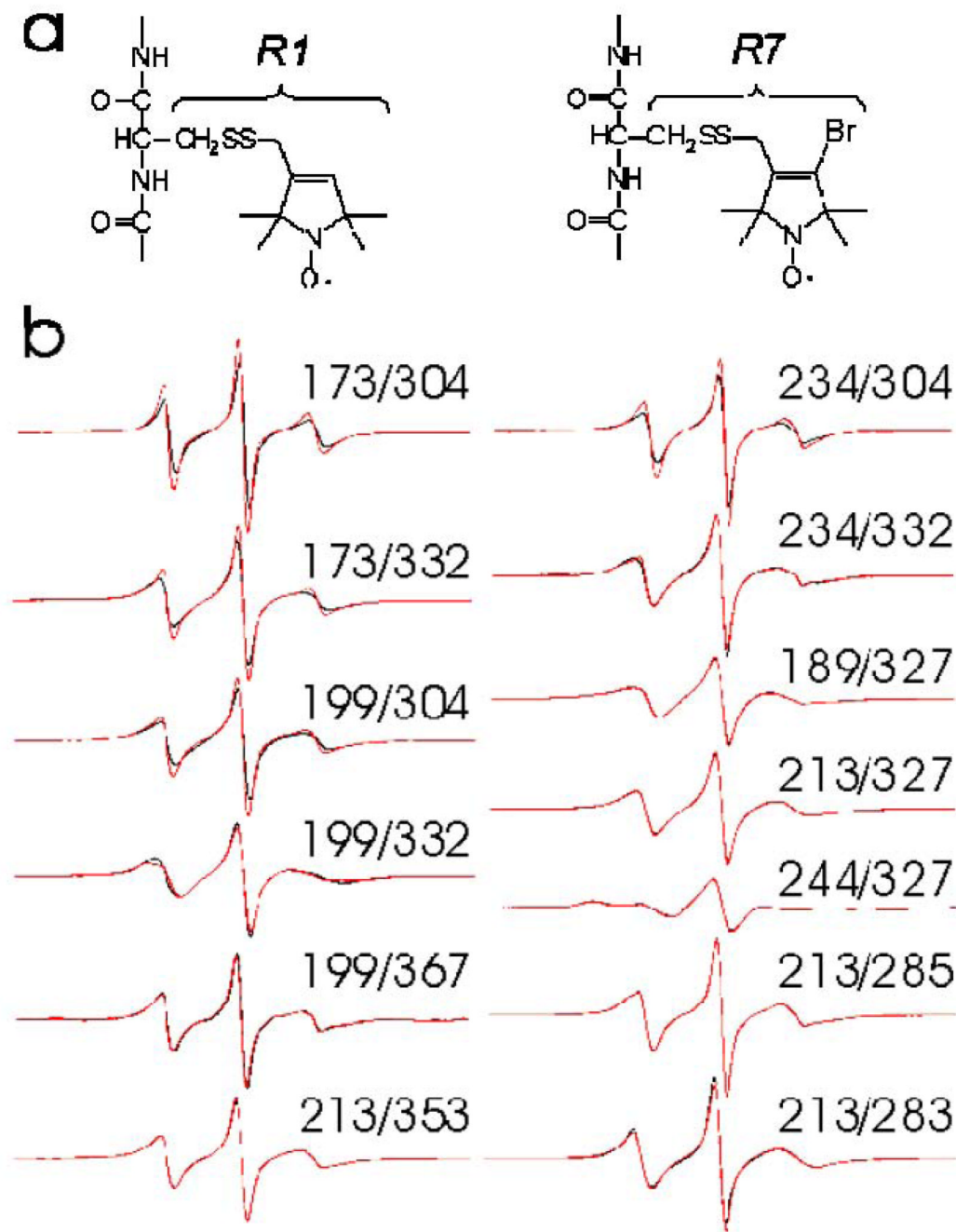


Figure 1. Models for synaptotagmin 1

(a) Synaptotagmin 1 is a membrane protein containing two C2 domains, which is anchored to the synaptic vesicle membrane by a single transmembrane helix. This model was built from models for the isolated C2A(PDB:1BYN) and C2B(PDB:1K5W) domains, which were connected with an unstructured linker using InsightII. (b) Crystal structure of the soluble fragment of synaptotagmin 1 (PDB:2R83). The C2A and C2B domains are shown in yellow and magenta.

**Figure 2. EPR spectra from syt1C2AB**

(a) R1 and R7 spin-labeled side chains that are obtained by derivatization of cysteine mutants of syt1C2AB. (b) X-band EPR spectra of thirteen R1 double labeled mutants of syt1C2AB where one label is in C2A and a second is in C2B. The black traces are spectra recorded in the presence of excess Ca²⁺ (1 mM) and the red traces are spectra recorded in the Ca²⁺-free state.

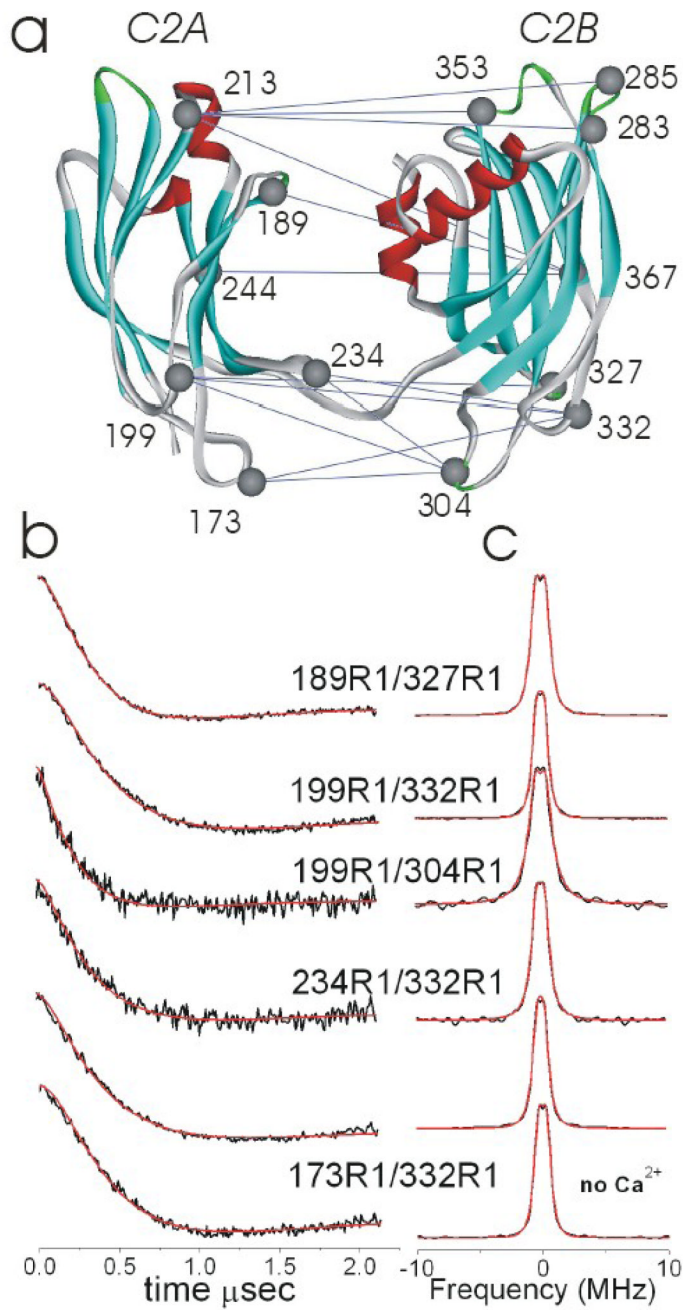


Figure 3. Distance measurements from C2A to C2B

(a) The soluble fragment of synaptotagmin 1 (syt1C2AB) containing both the C2A and C2B domains and encompassing residues 156 to 418. Thirteen sets of residue pairs were used for double electron-electron resonance (DEER) distance measurements. **(b)** Subtracted DEER signals obtained from the indicated labeled pairs in the presence of 1 mM Ca^{2+} , and **(c)** the corresponding Pake function obtained by deconvolution. The corresponding Pake functions that best fit the DEER data are shown in the red traces. The 173R1/332R1 mutant pair is also shown in the Ca^{2+} -free condition.

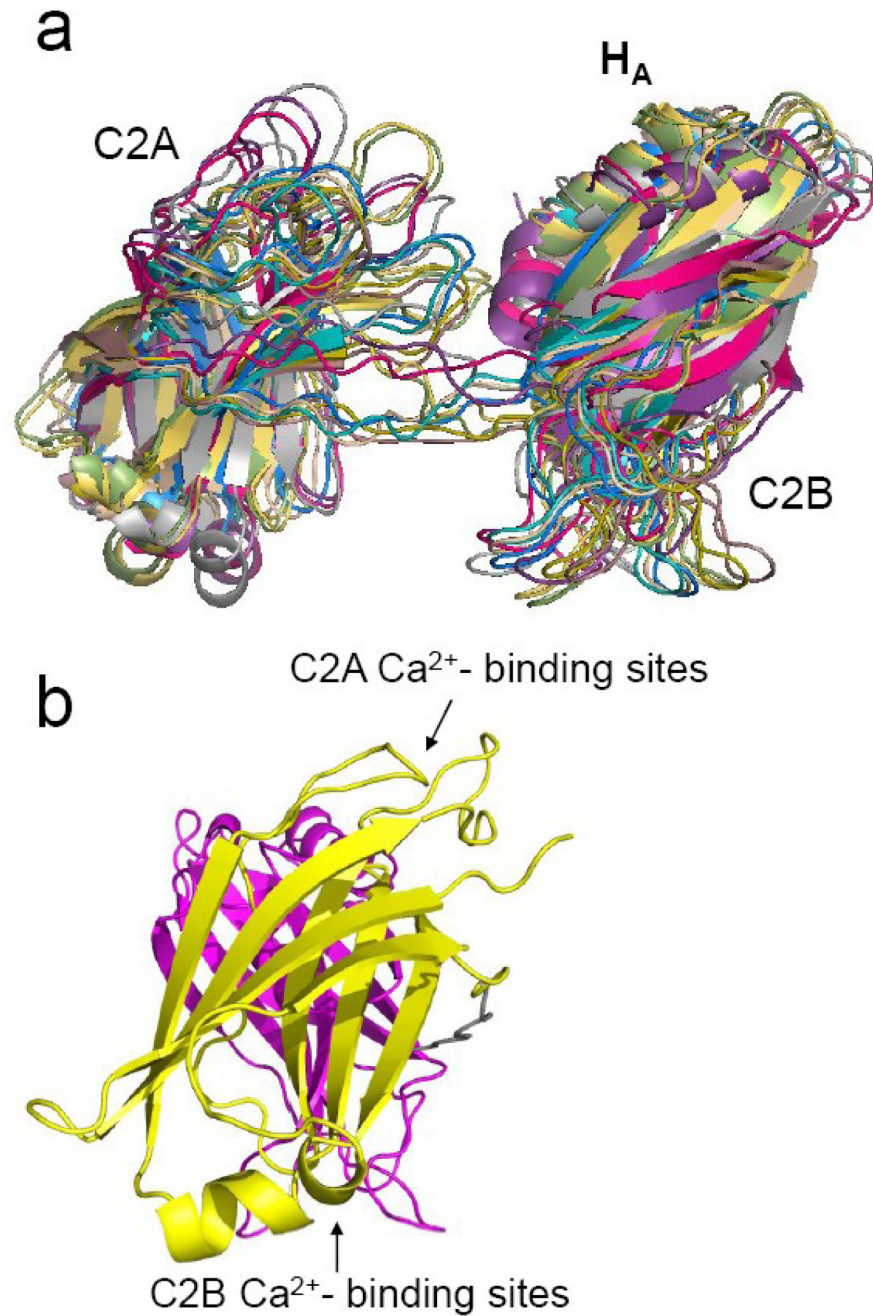


Figure 4. Solution structures of syt1C2AB with Ca^{2+} obtained by simulated annealing

(a) An alignment of the 10 lowest energy structures from the simulated annealing incorporating the distance restraints in Table 1 with Xplor-NIH and allowing the region linking C2A and C2B (residues 266 to 272) to be flexible³⁶. The RMSD for these aligned structures is approximately 5.0 Angstroms. (b) Average of the 20 lowest energy structures shown end on (C2A is in yellow, C2B in magenta). The β-sheet regions of both domains are not perfectly co-linear but are tilted by about 70 degrees.

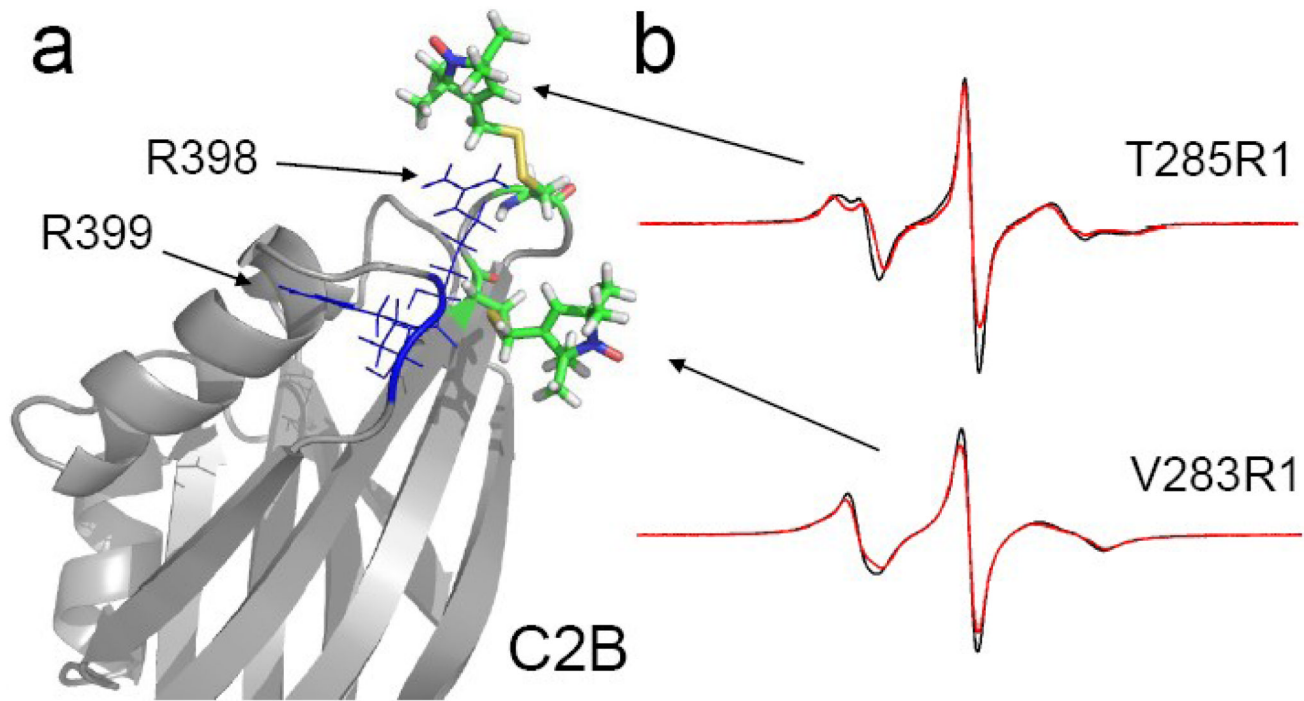


Figure 5. Location of R1 labels on C2B, opposite the Ca^{2+} -binding loops

a) Two spin labels V283R1 and T285R1 were engineered into a region where two highly conserved arginine residues, R398 and R399 are proposed to interact with an opposing bilayer surface¹⁷. **b**) The EPR spectra for T285R1 and V283R1 in the absence (black trace) and presence (red trace) of POPC:POPS bilayers with saturating levels of Ca^{2+} . These spectra are indicative of rapid anisotropic label motion, and T285R1 shows a noticeable change upon membrane association that may be due to a decrease in the apparent hyperfine coupling.

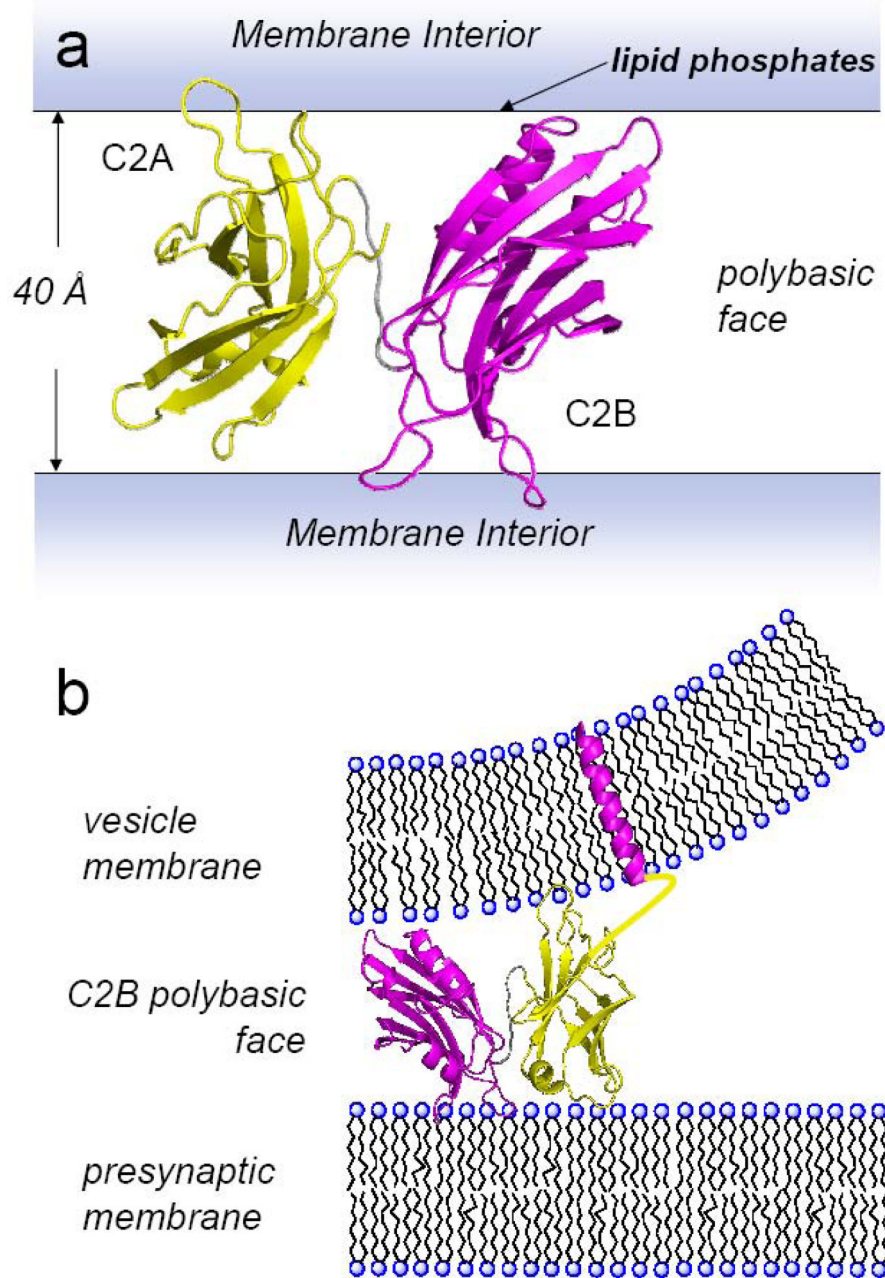


Figure 6. Structure for syt1C2AB obtained by docking syt1C2AB to two bilayer planes

a) Lowest energy structure obtained by simulated annealing using inter-domain depth restraints and point-to-plane depth restraints. For each domain loops 1 and 3 are either buried into or contact the membrane interface. The alignment of the two domains places the polybasic strand of C2B away from the bilayer interface. **b)** Docking of syt1C2AB showing the position of C2A and C2B on the vesicle and target membranes, respectively. The position of syt1 at the focal site of fusion may be influenced by the distribution of highly charged lipids, such as PI(4,5)P₂, as well as by interactions of the polybasic face of C2B with the SNAREs. C2A is shown in yellow, C2B in magenta.

Table 1Distances (in Angstroms) obtained by DEER between C2A and C2B.[†]

C2A/C2B mutant	[*] Ca ²⁺	EGTA	[*] POPC:POPS
M173R1/V304R1	39±9	41±13	38±19
M173R1/K332R1	45±10	46±9	46±11
R199R1/V304R1	37±16	39±15	40±14
R199R1/K332R1	46±9	47±8	46±8
R199R1/I367R1	43±5	44±5	--
F234R1/V304R1	33±11	36±9	27±18
F234R1/K332R1	42±14	41±13	44±12
K189R1/K327R1	43±12	--	43±11
K213R1/K327R1	50±7	--	48±5
K213R1/V283R1	60±18		61±16
K213R1/T285R1	60±10		62±12
K213R1/Q353R1	54±13		56±15
K244R1/K327R1	41±11	--	45±10

[†] Distances represent Gaussian fits to the distance distributions determined using the program DEER analysis⁴⁶. The range given represents the standard deviation to the Gaussian fit. For most of the distances, the uncertainty in the distance is estimated to be approximately 2 to 3 Angstroms, and the uncertainty in the distribution is approximately 30%. The R199R1/I367R1 pair labeled poorly, and the distances measured from K213R1 are long. For these five mutant pairs, there is approximately a 4 Å distance uncertainty and a 50% uncertainty in the distribution.

* Data for the Ca²⁺-bound aqueous and the membrane-bound forms of syt1C2AB were used to determine a family of structures using simulated annealing.

Table 2

Point-to-plane depth restraints used for membrane docking.

mutant	Φ	distance (Å)	Range (Å)
L171R1	-1.9	-4.0	$-43.0 < x < 0.0$
M173R1	+0.8	+7.8	$+6.9 < x < +8.6$
G174R1	+0.5	+6.9	$+6.7 < x < +7.2$
[†] K189R1	-1.8	-3.0	$-43.0 < x < -2.1$
L202R1	-2.5	-22.0	$-43.0 < x < -5.0$
F231R1	-1.4	0.0	$-4.0 < x < +2.4$
F234R1	-0.1	+5.2	$+4.9 < x < +5.5$
K236R1	-0.3	+4.6	$+3.9 < x < +5.2$
I239R1	-1.5	-0.6	$-3.0 < x < +1.1$
[†] V283R1	-1.9	-4.0	$-43.0 < x < -3.0$
[†] T285R1	-1.4	0.0	$-4.0 < x < +2.4$
K300R1	-1.7	-2.1	$-5.4 < x < 0$
V304R1	-0.4	+4.3	$+3.6 < x < +4.9$
G305R1	+0.8	+7.8	$+7.2 < x < +8.3$
G306R1	+0.3	+6.4	$+5.5 < x < +7.2$
K327R1	-2.2	-10.6	$-43.0 < x < -5.4$
T334R1	-2.2	-10.6	$-43.0 < x < -7.3$
I367R1	-2.1	-7.3	$-43.0 < x < -2.1$
G368R1	+0.6	+7.2	$+6.9 < x < +7.5$
K369R1	-1.2	+1.1	$0.0 < x < +2.0$
N370R1	-2.3	-21.1	$-43.0 < x < -5.4$

Distances were determined from measured values of Φ as described elsewhere^{9; 50}. The distances represent the distance from the nitrogen atom on the nitroxide R1 side chain to the plane that defines the average position of the lipid phosphates. Negative distance numbers correspond to labels on the aqueous side of the phosphate plane, positive numbers represent labels that lie on the hydrocarbon side. Most of the point-to-plane distances given in this table were reported previously and were determined using Ni(II)EDDA and oxygen collision parameter¹⁰. Values for three sites were determined here ([†]). The distance ranges are based upon the error in Φ and the form of the calibration curve (see Methods).